

GEONEUTRINO OSCILLATIONS APPROACH TO  
DISCRIMINATE DISTRIBUTIONS OF HPE IN  
THE EARTH'S MANTLE USING THE MONTE  
CARLO TECHNIQUE.

DANIEL FELIPE FORERO SÁNCHEZ

ADVISOR: JUAN CARLOS SANABRIA PhD.

Co-ADVISOR: JEAN-BAPTISTE TARY PhD.

This dissertation is submitted for the degree of  
**GEOSCIENTIST**



Geosciences Department  
Faculty of Science  
Universidad de Los Andes  
Bogotá, Colombia  
November 15, 2017



Dedicated to my little niece, Ana María, without whom this thesis would have been finished much, much earlier.

# Contents

<b>1</b>	<b>Introduction</b>	<b>2</b>
<b>2</b>	<b>Relevance of the Study</b>	<b>4</b>
<b>3</b>	<b>Distribution of Radioactive Elements</b>	<b>5</b>
3.1	Distribution of Elements . . . . .	5
3.2	Relative Abundances . . . . .	6
3.2.1	Bulk Silicate Earth . . . . .	6
3.2.2	Crust . . . . .	7
3.2.3	Mantle . . . . .	7
<b>4</b>	<b>Radioactivity</b>	<b>9</b>
4.1	Overview . . . . .	9
4.2	Types of radioactive decay . . . . .	10
4.2.1	Alpha decay . . . . .	10
4.2.2	Gamma decay . . . . .	10
4.2.3	Beta decay . . . . .	10
4.3	Decay Chains . . . . .	12
4.4	(Anti)Neutrino emission . . . . .	12
<b>5</b>	<b>Neutrino Physics</b>	<b>14</b>
5.1	Time evolution . . . . .	15
5.1.1	Three-flavor exact . . . . .	15
5.1.2	Two-flavor approximation . . . . .	16
<b>6</b>	<b>The Model</b>	<b>18</b>
6.1	Modelling the Earth . . . . .	18
6.2	Modelling the Flux . . . . .	18
6.2.1	The Flux Integral . . . . .	18
6.2.2	Survival Probability . . . . .	19
6.3	UANdINO . . . . .	20
6.4	Terrestrial Neutrino Units . . . . .	20

<b>7 Results</b>	<b>24</b>
7.1 UANdINO . . . . .	24
7.2 Flux simulation . . . . .	25
<b>8 Analysis</b>	<b>28</b>
<b>9 Conclusions</b>	<b>31</b>
9.1 Further Problems . . . . .	31
<b>References</b>	<b>33</b>

# List of Figures

4.1	Feynman diagram for $\beta^+$ process. . . . .	11
4.2	Feynman diagram for $\beta^-$ process. . . . .	11
4.3	Feynman diagram for electron capture. . . . .	12
4.4	Geoneutrino energy spectrum from [2]. . . . .	13
5.1	Survival probability in function of the distance to the detector obtained through the two-flavor approximation. Taken from reference [2]. . . . .	17
6.1	Various plots showing different attributes of class <code>RingNode</code> . .	21
6.2	Top: Plot of probabilities as given by UANdINO. Bottom: Plot from reference [11]. These are neutrino transition ( $\mu \rightarrow e$ ) probabilities for a constant density profile. Details in ref. [11]. . . . .	22
6.3	Neutrino transition and survival probabilities for constant-density profile and their sum, results from UANdINO. . . . .	23
7.1	Left: Density path in energy units for antineutrinos ( $\bar{\mathcal{A}}$ ). Right: Survival probability for different energies. . . . .	24
7.2	Abundance model and flux contribution for U and Th in the two-layer HPE distribution model. . . . .	27
8.1	Mantle fluxes due to $U$ (left) and $Th$ (right), compared with those given in reference [13]. . . . .	29
8.2	Geoneutrino signal expected from the mantle for the different models and the expected signal from detectors according to reference [8]. . . . .	29
8.3	Total geoneutrino flux expected from the different models. Triangles are still two-layer and squares, uniform HPE distributions. Colored bands correspond to signals measured by the detectors according to reference [8]. . . . .	30

# List of Tables

6.1	Values of the different constants in equation 6.1. Taken from reference [13]. . . . .	19
7.1	First results on geoneutrino flux from the mantle (in $cm^{-2}/\mu s$ ) for different BSE and HPE distribution models. Using average probability from two-flavor approximation. . . . .	25
7.2	Results on geoneutrino flux from the mantle (in $cm^{-2}/\mu s$ ) for different BSE and HPE distribution models. Using UANdINO probability. . . . .	25
7.3	Whole SE results on geoneutrino flux (TNU) for different BSE and HPE distribution models, using two-flavor approximation for survival probabilities. . . . .	26
7.4	Whole SE results on geoneutrino flux (TNU) for different BSE and HPE distribution models, using UANdINO's results for survival probabilities. . . . .	26
8.1	Experimental values for geoneutrino flux in detectors Borexino and KamLAND. Taken from reference [8]. . . . .	28



# Preface

## Acknowledgements

# 1

## Introduction

*“I have done something very bad today by proposing a particle that cannot be detected”*

– Wolfgang Pauli

Fortunately, Pauli was a bit wrong in this one, not because of the prediction of the particle, but for the fact that we were, eventually, able to detect these particles called neutrinos. They have been proven to be some of the most bizarre mysteries of our universe due to their unique physical behavior and properties. Their low interaction and oscillation phenomena makes them, not only difficult to see, but also useful in some areas of study. The present work focus on how can we exploit these characteristics to withdraw useful information of some physically unreachable places, for example, the Earth’s interior.

In this work, I will be simulating the geoneutrino flux from an azimuthally symmetrical Earth, taking into account the PREM density model (reference [1]). This simple Earth’s structure model plus the usage of an exact solution for the antineutrino oscillation in the matter (of reference [11]) are a “simple enough” model of the problem that will allow to draw some conclusions on the Heat Producing Element distribution in the mantle and evaluate the usefulness of the complete, exact treatment of neutrino oscillations in this context.

The second chapter briefly describes the relevance of this study. Then, the distribution of radioactive elements in the Earth is discussed, first, through an overview of the Goldschmidt classification of chemical elements, and then, showing the abundances of the relevant isotopes in each of the three main layers of the planet.

In chapter 4 the phenomena of radioactivity is explained, as well as the different types of radioactive decay. The relevant decay chains are shown, along with the geoneutrino spectra for the  $\beta^-$  decay.

Chapter 5 is an overview of the neutrino physics. This includes a short description of the oscillation phenomena, as well as introducing two different

methods of calculating the survival probability for an electron antineutrino: the exact, three-flavor matter oscillation used in this study and the two-flavor matter oscillation used in some previous studies.

Then, in chapter 6, the details of the modeling, including some aspects of the programs written, are given. This is considered a crucial part of this work as it will be the base of any further study to be done.

The chapter 7, the results of the simulations are given, while in chapter 8 they are discussed. In chapter 9 some conclusions on this project are given, as well as the further problems on the field.

## 2

# Relevance of the Study

The Earth is a complex system, in which we are rarely able to directly probe some characteristics, such as the composition of the deep Earth. In this aspect, one usually uses the available information in the surface, such as the composition of xenoliths, or seismic information, directly related to rheology, from which some relations to the composition can be withdrawn. Inspired by the latter, we can say that the development of indirect methods to probe the deep Earth is important, given the impossibility of directly doing it.

Neutrino geoscience is a relatively new field in geophysics and some applications of it are the estimation of radiogenic heat flux (Urey ratio) and testing HPE distributions or BSE models, nevertheless, being a new field as it is, the full potential of neutrino geoscience is yet to be discovered.

In order to develop reliable studies that involve (anti)neutrino oscillations through different variable densities, the appropriate computational tools must be developed. Thus, this study includes the development of UANDINO, the Uniandes ANtineutrINO Oscillation calculator. This is a GSL (reference [3]) based software dedicated to provide an exact calculation of transition and survival probabilities for an (anti)neutrino traveling through a varying density path with energy  $E_\nu$ . Along with it, other side programs were developed for modeling the Earth's structure.

# 3

# Distribution of Radioactive Elements

## 3.1 Distribution of Elements

A first, basic approach to understanding the distribution of elements in the Earth was given by Goldschmidt [5], who developed a classification system for the chemical elements. This classification is, in a nutshell, *lithophile* or oxygen-loving elements tend to remain in the uppermost part of the solid planet; *siderophile* or iron-loving elements, tend to be close to the nucleus and are not attracted to oxygen, unlike the lithophiles. The *chalcophile* elements are sulfur-loving and, thus, do not like the deep Earth. Finally, the *atmophile* elements are those who like to be in the atmosphere.

There are many radioactive isotopes in the Earth, which are, basically, atoms so heavy that they are unstable, and go through different processes to reach a more stable state. This will be the topic of chapter 4. Most of these heavy elements are classified as lithophiles. We are particularly interested in some isotopes that dominate the geoneutrino production (99% of production) [8], these are  $^{40}K$ ,  $^{235}U$ ,  $^{238}U$  and  $^{232}Th$ .

Within each of the groups given by Goldschmidt and briefly described here, there is other classification that discriminates elements based on their condensation temperature. The elements with a high value of this parameter are called *refractory* while the ones with a lower one are called *volatile*. Let us then picture the scenario of the formation of the Earth. About 4500 *Gyr* ago, the solar system and the Earth were being formed, the latter through planetary accretion, this means, a hot, undifferentiated mass of molten rock that is slowly cooling down, the consequences of this are, first of all, density differentiation, that causes the heavier elements to accumulate near the center of mass, thus, forming the nucleus. It also causes the elements to con-

dense, so the refractory ones, are quickly trapped into the Earth, making it possible to infer the initial abundances of these elements in the primitive Earth by looking at their abundances in different meteorites. On the other hand, volatile elements will not be trapped so easily or quickly, instead, there is a possibility that these elements have escaped the primitive Earth while it was hotter; the gases are extremely volatile, while there are other elements, like potassium (whose relevance will become obvious in the following sections) that are moderately volatile.

I have mentioned that the cooling down of the primitive Earth, lead to density differentiation in layers, causing the layered structure of the planet. The less-dense melt that ascended all the way up made up the crust, and is enriched in lithophile elements such as  $U$ ,  $Th$ ,  $K$ . Nevertheless, there is still a large amount of these elements in the mantle.

## 3.2 Relative Abundances

This section is devoted to discuss the different views on the distribution of the radioactive isotopes, in depth, quantitatively. There are two main discussions to be considered; first, the average composition of the Bulk Silicate Earth (BSE) and, second, the distribution of Heat Producing Elements (HPE) in the mantle.

### 3.2.1 Bulk Silicate Earth

In the first place, we shall define the BSE as the “average” Earth composition when excluding the nucleus, in other words, an average between mantle and crust. Three main ideas on the BSE composition have arisen through the years and each one of them relies on different, valid, arguments.

The first model is the *geochemical*, that as the name suggests, is based in geochemical arguments to give values to the abundances and abundance ratios of elements in the planet. McDonough [9] analyzed peridotite samples in order to infer the BSE average compositions. Reference [9] reports values of  $A_{Th}^{BSE} = 79.5 \text{ ppb}$ ,  $A_K^{BSE} = 240 \text{ ppm}$  and  $A_U^{BSE} = 20.3 \text{ ppb}$ , while reference [13] reports  $A_{Th}^{BSE} = 80 \pm 13 \text{ ppb}$ ,  $A_K^{BSE} = 280 \pm 60 \text{ ppm}$  and  $A_U^{BSE} = 20 \pm 4 \text{ ppb}$  for this BSE model, note that both references are in agreement.  $A_X^Y$  stands for the abundance of element  $X$  in reservoir  $Y$ .

The second model is the *geodynamical*. This model is based on the current measurements of the Earth’s heat flow and assumes that the fraction of this heat due to radioactive decay is higher than the fraction due to secular cooling of the planet. In reference [13], the reported values of the abundances

are  $A_{Th}^{BSE} = 140 \pm 14 \text{ ppb}$ ,  $A_K^{BSE} = 350 \pm 35 \text{ ppm}$  and  $A_U^{BSE} = 35 \pm 4 \text{ ppb}$ . This model has particularly high values of  $A_X^Y$  due to the assumption that the majority of the flux is product of radioactivity.

The third and final model is the *cosmochemical*. It relies on the analysis of enstatite chondrites to infer the BSE composition, under the argument that this abundances specially the iron one, will easily explain the presence of the core, as explained in reference [8]. Reference [13] reports the following values relevant to this project:  $A_{Th}^{BSE} = 43 \pm 4 \text{ ppb}$ ,  $A_K^{BSE} = 146 \pm 29 \text{ ppm}$  and  $A_U^{BSE} = 12 \pm 2 \text{ ppb}$ .

In this study, I will compare the results for geoneutrino measurements for the different BSE models presented above.

### 3.2.2 Crust

The relative abundance of HPE in the crust has been the object of various studies ([6, 10, 12, 14, 15]) among which, for this project, I chose reference [6]. In this article, the authors develop a reference Earth model for the HPE, based on geochemical analysis performed on different rocks and following the CRUST 2.0 model for crustal thickness and properties. The values given are  $A_U^C = 453.19_{-0.25}^{+0.29} \text{ ppb}$  and  $A_{Th}^C = 1940.64_{-0.89}^{+1.56} \text{ ppb}$ , from reference [6].

### 3.2.3 Mantle

The abundance of isotope  $X$  in the mantle,  $A_X^M$ , is calculated from the values reported above for  $A_X^{BSE}$  and  $A_X^C$  and the mass balance [13]:

$$m_{BSE}A_X^{BSE} = m_C A_X^C + m_M A_X^M, \quad (3.1)$$

that is, the total mass of isotope  $X$  is the sum of the mass in the crust and the mantle. The mass of reservoir  $Y$ ,  $m_Y$ , is calculated through integration of the mass density of the Earth given by the PREM model in reference [1], the details of the method will be given in chapter 6.

Additionally, the mantle structure is currently debated. Two of the most accepted models are the uniform mantle and the two-layer (EL-DL) mantle. The former consists in uniformly distributed HPE over the mantle, thus, the abundance in every point will be given by equation 3.1. The latter, in which EL and DL stand for enriched and depleted layer, respectively, consists in two layers of slightly different HPE abundances. The motivation for this is that the difference between the types of basalts (OIB, MORB, etc.) is thought to be caused by the differentiation of the mantle into two chemically distinct layers, an enriched layer and a depleted one, respect to lithophile elements. The enriched layer is said to constitute the lowermost

10% in mass of the bulk mantle [13]. The abundance in these two layers is also calculated using a relation similar to equation 3.1.

# 4

# Radioactivity

## 4.1 Overview

Radioactivity is the phenomenon in which a parent isotope turns into a daughter isotope, with different characteristics, through the emission of a particle.

The history of radioactivity goes back to 1896, when H. Becquerel discovered that a uranium sample emitted some kind of penetrating radiation similar to the X rays (discovered earlier that year). In the following years, three different types of emissions were identified: alpha ( $\alpha$ ), beta ( $\beta$ ) and gamma ( $\gamma$ ). The nature of each of these emissions was identified through the years, concluding that  $\alpha$ -particles correspond to  ${}^4He$  nuclei,  $\beta^\pm$ -particles correspond to  $e^\pm$  (electrons or positrons) and  $\gamma$ -particles are nothing but high energy photons.

Rutherford discovered that radioactive phenomena was linked directly with the nucleus (size  $\sim 1 \text{ fm}$ ) of a given isotope, thus, it is an entirely quantum phenomenon.

The overall radioactive phenomena are described by a rather simple mathematical approach given the statistical behavior of the phenomena (which is a result, and evidence of how “quantum”it is). Given  $N$  parent isotopes in a sample at a given time  $t$  and assuming no more are added, the rate of decay ( $dN/dt$ ) is proportional to  $N$  [7]

$$\frac{dN}{dt} = -\lambda N \quad (4.1)$$

That, upon integration becomes

$$N(t) = N_0 \exp(-\lambda t) \quad (4.2)$$

Where  $N_0$  corresponds to the number of parent isotopes at time  $t = 0$  and  $\lambda$  is called the decay constant and is unique for every isotope.

This simple model has been key to the use of the radioactive isotopes to, for

example, date rocks or organisms [7].

## 4.2 Types of radioactive decay

Let us now go deeper into the theory of the radioactivity, that is, briefly describe the different types of radioactive decays since not all of them produce antineutrinos, and these are the particles that concern this text.

### 4.2.1 Alpha decay

The theory of the alpha decay is rather simple. The  $\alpha$ -particles are confined in a finite potential well (the nucleus  $X$ ) and will, as expected, have a certain probability of tunneling said barrier. When this happens, the  $\alpha$ -particle will escape and leave a “new” (daughter) nucleus  $X'$  [7]. The process may be written as



Where  $A$  is the atomic mass number,  $Z$  is the atomic number and  $N$  is the charge.

This decay involves both strong (nuclear) interactions and electromagnetic interactions since the potential well is given by confinement due to strong interaction between nucleons and the barrier has a decaying-exponential side, given by the Coulomb potential.

### 4.2.2 Gamma decay

Gamma decay is similar to the common electromagnetic emission due to atomic transitions, in fact, it is produced when a metastable state of an isotope decays into a more stable state through the emission of high energy photons. It should be noted that, in this case, no change in  $A$  or  $N$  is produced. These metastable states are common daughter isotopes to  $\alpha$  and  $\beta$  decays.

Lifetimes for this kind of process is generally short, taking only fractions of a second to decay while some  $\alpha$ -decaying isotopes may have half-lives of the order of  $10^3$  yr.

### 4.2.3 Beta decay

This type of decay can be considered to be more complex than the other two, as it responds to more complicated underlying physics: the weak interaction. It consists in a set of semileptonic processes (that involve both leptons and hadrons) that will be described below.

- Positive Beta decay:

$$p \rightarrow n + e^+ + \nu_e \quad (4.4)$$

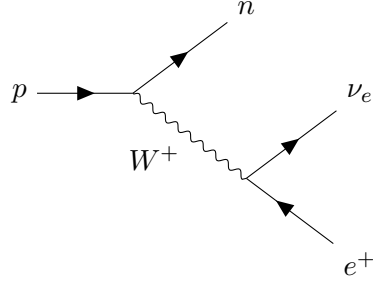


Figure 4.1: Feynman diagram for  $\beta^+$  process.

- Negative Beta decay:

$$n \rightarrow p + e^- + \bar{\nu}_e \quad (4.5)$$

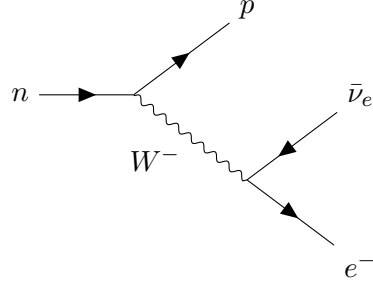


Figure 4.2: Feynman diagram for  $\beta^-$  process.

- Electron capture:

$$p + e^- \rightarrow n + \nu_e \quad (4.6)$$

Note that in all these processes new particles are created in the nucleus, which is a consequence of the weak interaction that rules them.

The particles labeled with  $\nu_e$  are electron neutrinos and were proposed by Pauli in order to solve the conundrum concerning the apparently continuous energy spectra of  $\beta$ -decay which is against the core of quantum mechanics, the inclusion of these particles in the energy spectrum of the decay made it discrete, thus, giving a solution to the problem [4].

For this project, we are strictly interested in the  $\beta^-$ -decay since it is the one that produces antineutrinos.

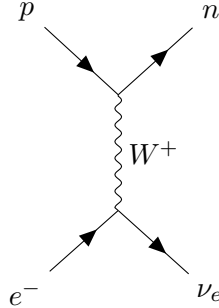


Figure 4.3: Feynman diagram for electron capture.

### 4.3 Decay Chains

Different isotopes in the Earth have decay chains that involve  $\beta^-$ -decay at some point, but there are a few ones that dominate the antineutrino production. The reader may have noticed that in chapter 3, I have said that the production of heat is dominated by  $^{238}U$ ,  $^{232}Th$  and  $^{40}K$ . Each isotope has a decay chain that includes some beta decays. These are summarized in the following equations.

$$^{238}U \rightarrow ^{206}Pb + 8\alpha + 8e^- + 6\bar{\nu}_e + 51.7MeV, \quad (4.7)$$

$$^{235}U \rightarrow ^{207}Pb + 7\alpha + 4e^- + 4\bar{\nu}_e + 46.4MeV, \quad (4.8)$$

$$^{232}Th \rightarrow ^{208}Pb + 6\alpha + 4e^- + 4\bar{\nu}_e + 42.7MeV, \quad (4.9)$$

$$^{40}K \rightarrow ^{40}Ca + e^- + \bar{\nu}_e + 1.31MeV, \quad (4.10)$$

$$^{40}K + e^- \rightarrow ^{40}Ar + \bar{\nu}_e + 1.505MeV. \quad (4.11)$$

Note that the processes shown in equations 4.10 and 4.11 have the same parent isotope, the former happens with a probability of 89.3% and the latter with the remaining 10.7%.

In equations 4.7 through 4.11, the particles  $\bar{\nu}_e$  are electron antineutrinos, also called geoneutrinos, in this context.

### 4.4 (Anti)Neutrino emission

As seen in the previous section, naturally produced antineutrinos from beta decay are called geoneutrinos. These are produced following a given spectrum [2], shown in figure 4.4. Figure 4.4 shows that the energy domain for

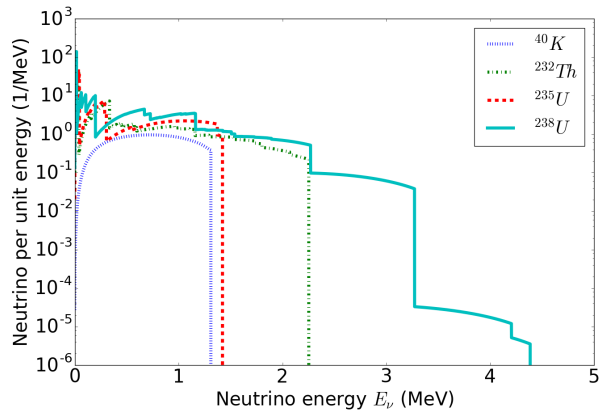


Figure 4.4: Geoneutrino energy spectrum from [2].

these particles is relatively low, this means that, in the light of reference [11], oscillations will not be of such importance because the transition or survival probabilities do not show a clear pattern in these energy scales. Nevertheless it is worth mentioning that resonances in the probabilities are present at higher energy scales.

# 5

## Neutrino Physics

This chapter is only an overview of the special physics that surrounds these particles, for a thorough explanation you should see reference [4] and for details on time evolution, reference [11].

Neutrinos are neutral leptons that interact weakly and are always produced in a given flavor eigenstate  $|\nu_\alpha\rangle$  with  $\alpha = e, \mu, \tau$ . In equations 4.4 to 4.6, all neutrinos are labeled  $\nu_e$  that stands for electron neutrino, this is because they are all associated with the “ordinary” matter which is composed by electrons, not tauons ( $\tau$ ) or muons ( $\mu$ ), which are other charged leptons, this is, electrically charged particles that lack color charge.

I just mentioned neutrinos are produced in flavor states, but these are not mass (energy) eigenstates and, since the Hamiltonian entirely controls the time evolution of a quantum system, the neutrinos will not evolve (travel) in these states but will rather oscillate between the real mass eigenstates which, as the name suggests, do have a definite (and unknown) mass, while flavor states are just a linear combination of them. This may be written as

$$|\nu_\alpha\rangle = \sum_{a=1}^3 U_{\alpha a}^* |\nu_a\rangle \quad (5.1)$$

Here, we have labeled  $|\nu_a\rangle$  the mass eigenstates, with  $a = 1, 2, 3$ .  $U_{\alpha a}^*$  is the matrix element of the transformation matrix  $U^*$  [11].

The matrix  $U^*$  is the complex conjugate of matrix  $U$ , called Pontecorvo-Maki-Nakagawa-Sakata (PMNS) matrix, that rules the mixing of the neutrinos and can be parametrized as shown in [11]

$$U = \begin{bmatrix} C_2 C_3 & S_3 C_2 & S_2 \\ -S_3 C_1 - S_1 S_2 C_3 & C_1 C_3 - S_1 S_2 S_3 & S_1 C_2 \\ S_1 S_3 - S_2 C_1 C_3 & -S_1 C_3 - S_2 S_3 C_1 & C_1 C_2 \end{bmatrix} \quad (5.2)$$

Where  $S_i \equiv \sin(\theta_i)$  and  $C_i \equiv \cos(\theta_i)$ . Parameters  $\theta_i$  are the vacuum mixing angles. Here we have assumed there is no charge-parity (CP) phase, thus,  $U = U^*$ .

## 5.1 Time evolution

### 5.1.1 Three-flavor exact

According to the principles of quantum mechanics, the Hamiltonian of a system described by the ket  $|\psi\rangle$  does define its time evolution according to

$$|\psi(t)\rangle = \exp(-i\hat{H}(t-t_0))|\psi(t_0)\rangle \quad (5.3)$$

In the case of the neutrinos, we know that they do not travel in flavor state but in mass states, then, we can write

$$|\nu_a(t)\rangle = \exp(-i\hat{H}_m(t-t_0))|\nu_a(t_0)\rangle \quad (5.4)$$

In this base, the Hamiltonian will be diagonal

$$\hat{H}_{m,\text{unperturbed}} = \begin{bmatrix} E_1 & 0 & 0 \\ 0 & E_2 & 0 \\ 0 & 0 & E_3 \end{bmatrix} \quad (5.5)$$

Inside matter, the Hamiltonian of the system is perturbed in the following way

$$\hat{V}_f = \mathcal{A} \begin{bmatrix} 1 & 0 & 0 \\ 0 & 0 & 0 \\ 0 & 0 & 0 \end{bmatrix} \quad (5.6)$$

Where  $\mathcal{A}$  depends on the density of the matter the neutrino is going through, and is defined as

$$\mathcal{A}(r) \approx \pm \sqrt{2} G_F \frac{\rho(r)}{m_N} \quad (5.7)$$

Here,  $G_F$  is the Fermi coupling constant,  $\rho(r)$  is the matter density and  $m_N$  is the nucleon mass.

The perturbation  $V_f$  ( $f$  stands for flavor base) only affects electron-flavored neutrinos because matter, as we see it, is electronic. Taking this into account, the perturbed Hamiltonian, in mass basis is

$$\hat{H}_m = \begin{bmatrix} E_1 & 0 & 0 \\ 0 & E_2 & 0 \\ 0 & 0 & E_3 \end{bmatrix} + U^{-1} V_f U \quad (5.8)$$

Introducing equation 5.8 into 5.4 we can get the time evolution operator  $\hat{U}_f$  as follows (reference [11]). Consider a  $N \times N$  matrix  $M$ , the exponential of the matrix is defined as  $\exp M = \sum_{n=0}^{\infty} \frac{1}{n!} M^n$ . Now, recall Cayley-Hamilton's theorem: given a matrix  $M$ , the characteristic polynomial is  $p(x) = \det(x - M) = \sum_{i=0}^N c_i x^i$  ( $c_N = 1$ ,  $p(x)$  is monic), the theorem implies that  $p(M) = 0$ , this means that

$$p(M) = 0 = M^N + c_{N-1} M^{N-1} + \cdots + c_0, \quad (5.9)$$

then,

$$M^N = -c_{N-1}M^{N-1} - \cdots - c_0, \quad (5.10)$$

therefore, if one wishes to calculate  $M^m$  for any  $m \geq N$ , it will be given by

$$M^m = k_{N-1}^{(m)} M^{N-1} + \cdots + k_0^{(m)}, \quad (5.11)$$

given that coefficients  $k_i^{(m)}$  are properly calculated. Knowing this, the exponential of the matrix

$$\exp M = \sum_{n=0}^{\infty} \frac{1}{n!} M^n = \sum_{n=0}^{N-1} a_n M^n \quad (5.12)$$

and this result is exact.

Then, the transition probability from an initial flavor  $\alpha$  state to a  $\beta$  one will be

$$P_{\alpha \rightarrow \beta} = |\langle \beta | \hat{U}_f | \alpha \rangle|^2. \quad (5.13)$$

Given a density profile  $\rho(\mathbf{r})$ , one can divide it into  $K$  slices (or steps) with constant  $\mathcal{A}$  and calculate the respective time evolution operators  $\hat{U}_{f,i}$  ( $i = 0, \dots, K$ ) and build a total operator  $\hat{U}_{f,total} = \prod_i \hat{U}_{f,i}$  with which total survival probability is calculated using relation 5.13.

### 5.1.2 Two-flavor approximation

Previous studies ([2, 8]) use the two-flavor approximation to neutrino oscillation. This takes into account that the  $\tau$  neutrino is so heavy that it is rarely produced. In this case, we may write (as explained in [2])

$$\hat{H}_m = \begin{bmatrix} E_1 & 0 \\ 0 & E_2 \end{bmatrix} + U^{-1} V_f U, \quad U = \begin{bmatrix} \cos \theta & \sin \theta \\ -\sin \theta & \cos \theta \end{bmatrix}, \quad (5.14)$$

This results in a perturbed hamiltonian of the form

$$\hat{H}_f = \begin{bmatrix} -\frac{\Delta m^2}{4E_\nu} \cos 2\theta + \mathcal{A} & \frac{\Delta m^2}{4E_\nu} \sin 2\theta \\ \frac{\Delta m^2}{4E_\nu} \sin 2\theta & \frac{\Delta m^2}{4E_\nu} \cos 2\theta \end{bmatrix} \quad (5.15)$$

In order to solve this matter oscillation case, a new  $U'$  matrix is proposed

$$U' = \begin{bmatrix} \cos \theta' & \sin \theta' \\ -\sin \theta' & \cos \theta' \end{bmatrix}, \quad (5.16)$$

where

$$\cos 2\theta' \equiv \frac{-2\mathcal{A}E_\nu/\Delta m^2 + \cos 2\theta}{\sqrt{(2\mathcal{A}E_\nu/\Delta m^2 - \cos 2\theta)^2 + \sin^2 2\theta}}, \text{ and} \quad (5.17)$$

$$\sin 2\theta' \equiv \frac{\sin^2 2\theta}{\sqrt{(2AE_\nu/\Delta m^2 - \cos 2\theta)^2 + \sin^2 2\theta}} \quad (5.18)$$

Then, the mass difference is

$$\Delta m'^2 = \sqrt{(2AE_\nu - \Delta m^2 - \cos 2\theta)^2 + (\Delta m^2)^2 \sin^2 2\theta}. \quad (5.19)$$

This theorem is the basis of the whole calculation  $\hat{U}_f$ , for the rest of the algebra, you should check reference [11].

The probability is then calculated as shown in 5.13 if one defines  $\hat{U} = \exp(i\hat{H}t)$ . This results in

$$P_{ee} = 1 - \sin^2 2\theta' \sin^2 \left( \frac{\Delta m'^2 L}{4E_\nu} \right), \quad (5.20)$$

where  $L$  is the traveled distance (with constant  $A$ ). These references argue that this probability is well averaged since the quantity  $L_{osc} = \pi \frac{4E_\nu}{\Delta m^2} \ll R$  (so  $\sin^2(\dots) = 0$ ,  $L_{osc}$  is therefore known as oscillation distance), this results in very “tight” oscillations (as illustrated in figure 5.1), for all paths in the Earth. Then,

$$\langle P_{ee} \rangle = 1 - \frac{1}{2} \sin^2 2\theta' = 0.55. \quad (5.21)$$

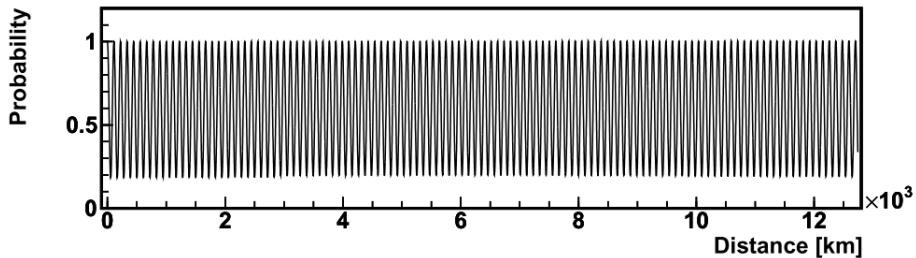


Figure 5.1: Survival probability in function of the distance to the detector obtained through the two-flavor approximation. Taken from reference [2].

On this project, I will adopt the exact solution to evaluate the real effect of a varying electron-density in the (anti)neutrino oscillation phenomena and how it will affect the detection.

# 6

## The Model

### 6.1 Modelling the Earth

In order to model the Earth, different assumptions were made. The biggest one is, probably, that the Earth is azimuthally symmetrical, nevertheless the model to be shown will allow for some complex radial and polar asymmetries.

All programs developed for the project are available in the repository <sup>1</sup> dedicated to it. Implementation is mainly done in C++, but a small part involving the probability calculations is done in Python.

For integrating, I use cylindrical coordinates, in which the  $z$  coordinate is, as usual  $z \in [-R, R]$ , where  $R = 6371\text{km}$  is Earth's Radius. The radial coordinate is called  $x \in [0, \sqrt{R^2 - z^2}]$ . Thus, we divide the Earth in rings, or nodes each ring will have a volume  $dV = 2\pi x dx dz$ . Computationally, the Earth is modeled by a  $500 \times 1000$  matrix of instances of the class `RingNode`, this type of data has a variety of attributes that will be introduced when necessary in this text.

The matrix itself is an attribute of the class `Planet`, that holds other attributes such as total mass, volume and fluxes. Figure 6.1 shows different attributes of `RingNode` class. These classes are defined in `earth_simul.h` and the respective implementation file `earth_simul.cpp`.

### 6.2 Modelling the Flux

#### 6.2.1 The Flux Integral

As in reference [13], the flux is given by the integral of equation 6.1.

$$\Phi_X(\mathbf{r}) = \frac{n_X \lambda_X}{4\pi} \int_{\Omega} \int_{\oplus} \frac{a_X(\mathbf{r}') \rho(\mathbf{r}') P_{ee}(\mathbf{r} - \mathbf{r}', E_\nu)}{|\mathbf{r} - \mathbf{r}'|^2} d^3 r dE_\nu \quad (6.1)$$

---

<sup>1</sup>[https://github.com/dforero0896/Physics\\_Monograph](https://github.com/dforero0896/Physics_Monograph)

	$^{238}U$	$^{232}Th$
$X$	0.9927	1
$M (u)$	238.051	232.038
$\tau_{1/2}$	4.468	14.05
$\lambda (10^{-18}/s)$	4.916	1.563
$n$	6	4

Table 6.1: Values of the different constants in equation 6.1. Taken from reference [13].

Here,  $n_X$  stands for the number of neutrinos produced in decay chain  $X$  (from equations 4.7 through 4.11),  $\lambda_X$  is the decay constant for each chain,  $a_X$  is the isotopic abundance at position  $\mathbf{r}'$ , defined as  $a_X = \frac{A_X X_X}{M_X}$ , where  $A$  is as defined in chapter 3,  $X_X$  is the isotopic ratio and  $M_X$  is the atomic mass. Then,  $\rho$  is the matter density and  $P_{ee}$  is the survival probability of the geoneutrinos produced at  $\mathbf{r}'$  with energy  $E_\nu$ , travelling towards  $\mathbf{r}$ . Finally, the factor  $\frac{1}{4\pi|\mathbf{r}-\mathbf{r}'|^2}$  accounts for the spherically divergent flux. The values used for these factors are shown in table 6.1. Integration should be done in domains  $\oplus$  (Earth) spatially and  $\Omega$ , shown in figure 4.4, for the energy. All these quantities are attributes to the class `RingNode`.

### 6.2.2 Survival Probability

The quantity  $P_{ee}$  depends on both the path ( $|\mathbf{r} - \mathbf{r}'|$ ) the geoneutrino takes, and the energy ( $E_\nu$ ) with which it is produced. The energy of these antineutrinos depends on the spectra ( $\frac{dn}{dE_\nu}$ ) in figure 4.4. The way of performing the integral over the energies is the following: for a given node in the matrix, the path to the detector is calculated, for this path and  $M = 300$  samples of energy, the survival probability ( $P_i$ ) is obtained. Then, for the same energies, the spectra is sampled, this results in  $M$  values  $f_i$ . Each is normalized as  $w_i = f_i / \sum_i f_i$ . These  $w_i$  are the weights corresponding to each probability. Finally the probability for each node is

$$P_{ee}(|\mathbf{r} - \mathbf{r}'|) = \sum_i w_i P_i. \quad (6.2)$$

There are three programs that handle this step: `raw_probs.cpp` that calculates the raw probabilities (as previously mentioned in section 5.1.1) for a node and writes them in the file `raw_probs.csv`, `prob_weight.cpp` that calculates the weights  $w_i$  for a node and exports them to a file `prob_weight.dat` and `prob_integrating.py` that is in charge of running the C++ programs for all node  $i, j$  in the Earth and calculating the “average” probability for

each one (equation 6.2) and writing them to file `probability_planet.csv`, which is used in the calculations of the flux.

It is worth mentioning that prior studies use an average probability given by approximating the two-flavor oscillation model (equation 5.21).

### 6.3 UANdINO

As stated before, UANdINO is a C++, GSL-based program that, given a density path and an (anti)neutrino energy, calculates the survival probability. It is entirely based on the work done in reference [11]. The development of this software was a crucial part of this work and the idea is that everybody, who needs it, is able to use it, therefore I decided to name it.

In order to test the functionality of the software, I reproduced some plots of said reference, this is shown in figure 6.2. I also checked that, being probabilities, all of them added up to one. This test is shown in figure 6.3.

### 6.4 Terrestrial Neutrino Units

Terrestrial Neutrino Units (TNU) is the usual unit used in (anti)neutrino experiments. TNU is defined as the number of interactions in one year when using a target of  $10^{32}$  protons and 100% detection efficiency. Reference [8] defines the conversion as follows, where  $S(X)$  is in TNU and  $\Phi_X$  is in  $cm^{-2}/\mu s$ .

$$S(^{232}Th) = 4.07\Phi_{Th} \quad (6.3)$$

$$S(^{238}U) = 12.8\Phi_U \quad (6.4)$$

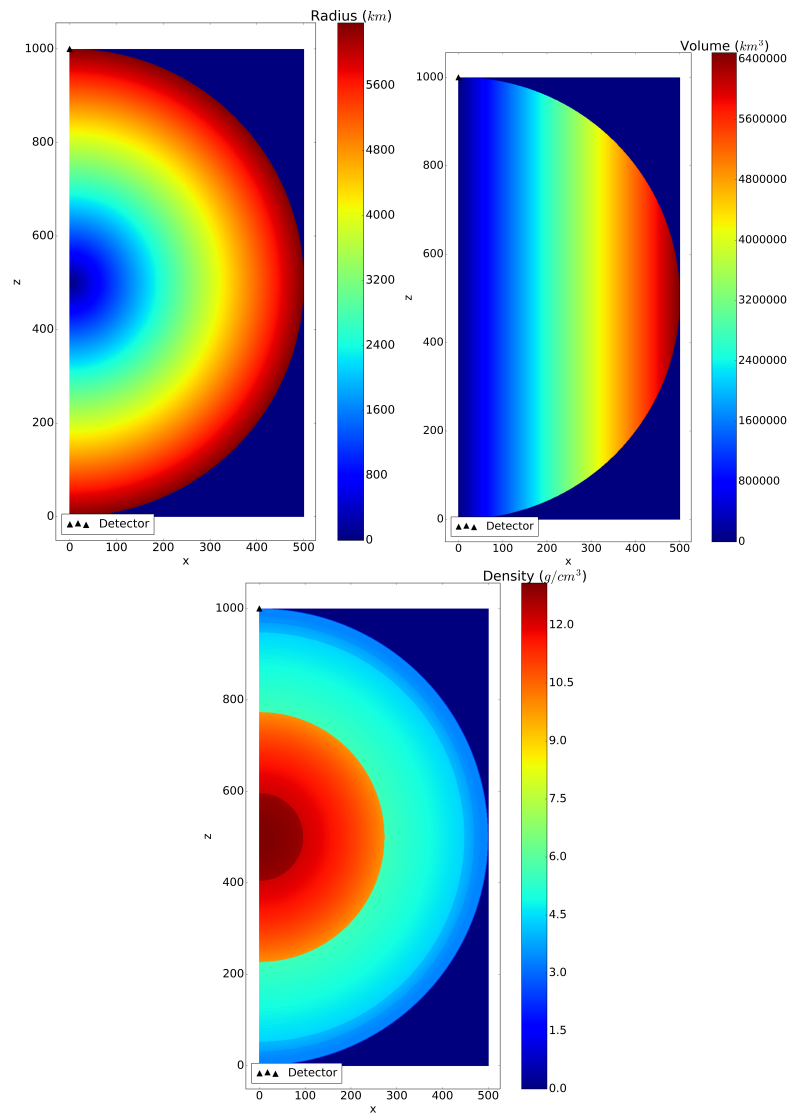


Figure 6.1: Various plots showing different attributes of class `RingNode`.

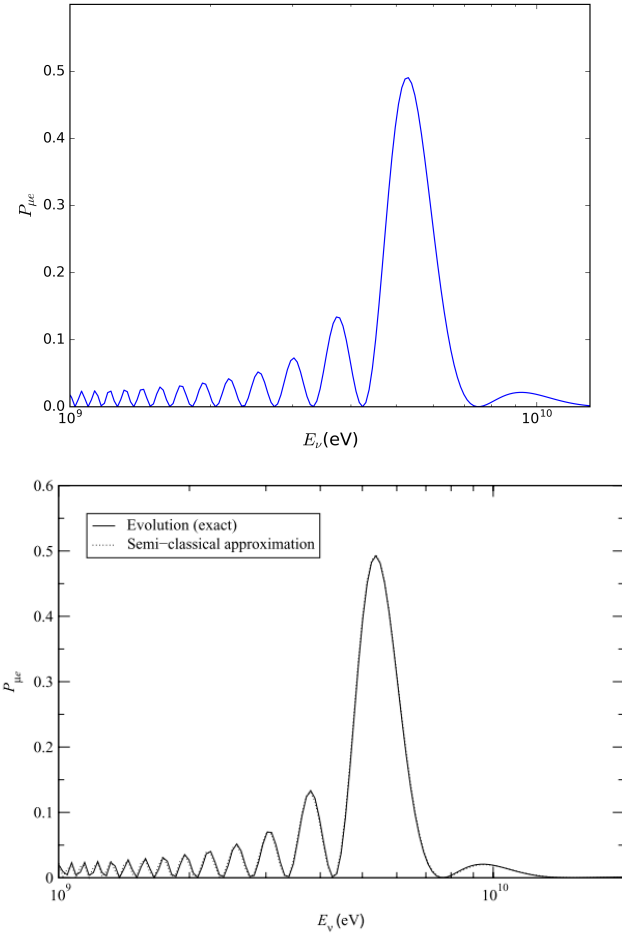


Figure 6.2: Top: Plot of probabilities as given by UAndINO. Bottom: Plot from reference [11]. These are neutrino transition ( $\mu \rightarrow e$ ) probabilities for a constant density profile. Details in ref. [11].

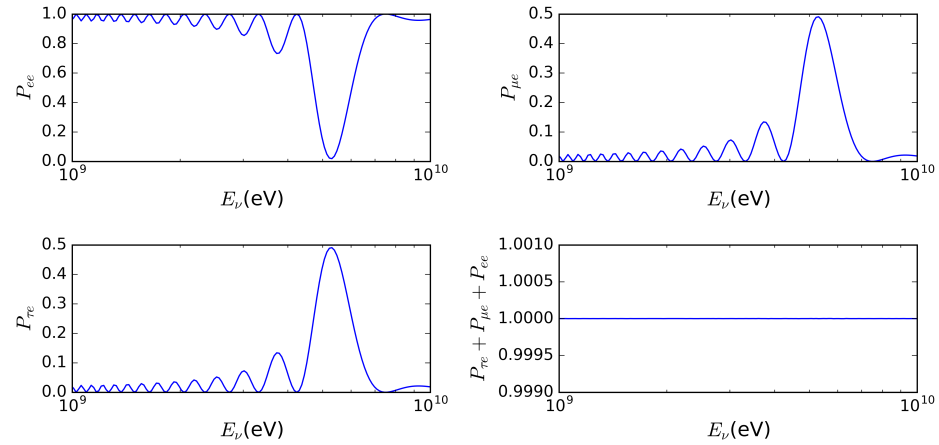


Figure 6.3: Neutrino transition and survival probabilities for constant-density profile and their sum, results from UAndINO.

# 7

# Results

## 7.1 UAndINO

The UAndINO run was programmed in a Python script that called it iteratively for each path and all energies. This run was made in the HPC cluster of the university and took 4 days. The results of this are rather controversial. The averaged survival probability, according to different references ([2, 8]) is  $\langle P_{ee} \rangle \approx 0.5 - 0.6$  while UAndINO leads to values of  $P_{ee}(\mathbf{r} - \mathbf{r}') \approx 0.99$  as shown in figure 7.1. [h]

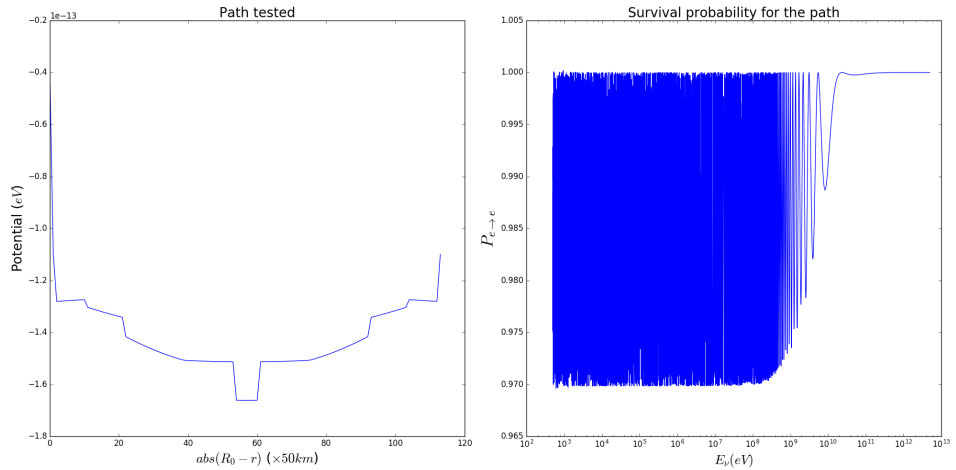


Figure 7.1: Left: Density path in energy units for antineutrinos ( $\mathcal{A}$ ). Right: Survival probability for different energies.

## 7.2 Flux simulation

Following the work in reference [13], a test with an average survival probability (from reference [8]) of  $\langle P_{ee} \rangle = 0.55$  from the two-flavor approximation, the different HPE distributions and BSE models was done, the results are shown in table 7.1. On the other hand, table 7.2 shows the results when using UANdINO's probabilities.

BSE Model \HPE distribution	Uniform		Two-layer	
	$\Phi_U$	$\Phi_{Th}$	$\Phi_U$	$\Phi_{Th}$
Geochemical	0.626	0.526	0.530	0.436
Cosmochemical	0.242	0.139	0.236	0.140
Geodynamical	1.345	1.158	1.079	0.917

Table 7.1: First results on geoneutrino flux from the mantle (in  $cm^{-2}/\mu s$ ) for different BSE and HPE distribution models. Using average probability from two-flavor approximation.

BSE Model \HPE distribution	Uniform		Two-layer	
	$\Phi_U$	$\Phi_{Th}$	$\Phi_U$	$\Phi_{Th}$
Geochemical	1.123	0.947	0.949254	0.781
Cosmochemical	0.435	0.250	0.426233	0.251
Geodynamical	2.414	2.078	1.930	1.640

Table 7.2: Results on geoneutrino flux from the mantle (in  $cm^{-2}/\mu s$ ) for different BSE and HPE distribution models. Using UANdINO probability.

The simulation allows for an inspection on the distribution of the flux, figure 7.2 shows the flux contribution to the total for both isotopes in the two-layer HPE distribution model.

One should note that, even though abundance of thorium is higher in every layer, its contribution to the total flux seems to be lower and less spatially spread. This can be attributed to the number of neutrinos  $n_X$ ,  $^{238}U$  produces 2 antineutrinos more in each decay, compared to  $^{232}Th$ .

For the whole silicate Earth and average probability the flux is shown in table 7.3.

But, when using the probabilities given by UANdINO for each node the results are quite different. These are shown in table 7.4.

BSE Model \HPE distribution	Uniform			Two-layer		
	$S_U$	$S_{Th}$	$S_{tot}$	$S_U$	$S_{Th}$	$S_{tot}$
Geochemical	5.357	15.046	20.403	4.968	13.876	18.844
Cosmochemical	3.797	10.074	13.870	3.777	10.081	13.858
Geodynamical	8.283	23.110	31.393	7.202	20.031	27.233

Table 7.3: Whole SE results on geoneutrino flux (TNU) for different BSE and HPE distribution models, using two-flavor approximation for survival probabilities.

BSE Model \HPE distribution	Uniform			Two-layer		
	$S_U$	$S_{Th}$	$S_{tot}$	$S_U$	$S_{Th}$	$S_{tot}$
Geochemical	9.617	27.010	36.627	8.909	24.881	33.79
Cosmochemical	6.816	18.086	24.902	6.780	18.098	24.879
Geodynamical	14.869	41.481	56.350	12.900	35.881	48.781

Table 7.4: Whole SE results on geoneutrino flux (TNU) for different BSE and HPE distribution models, using UANdINO's results for survival probabilities.

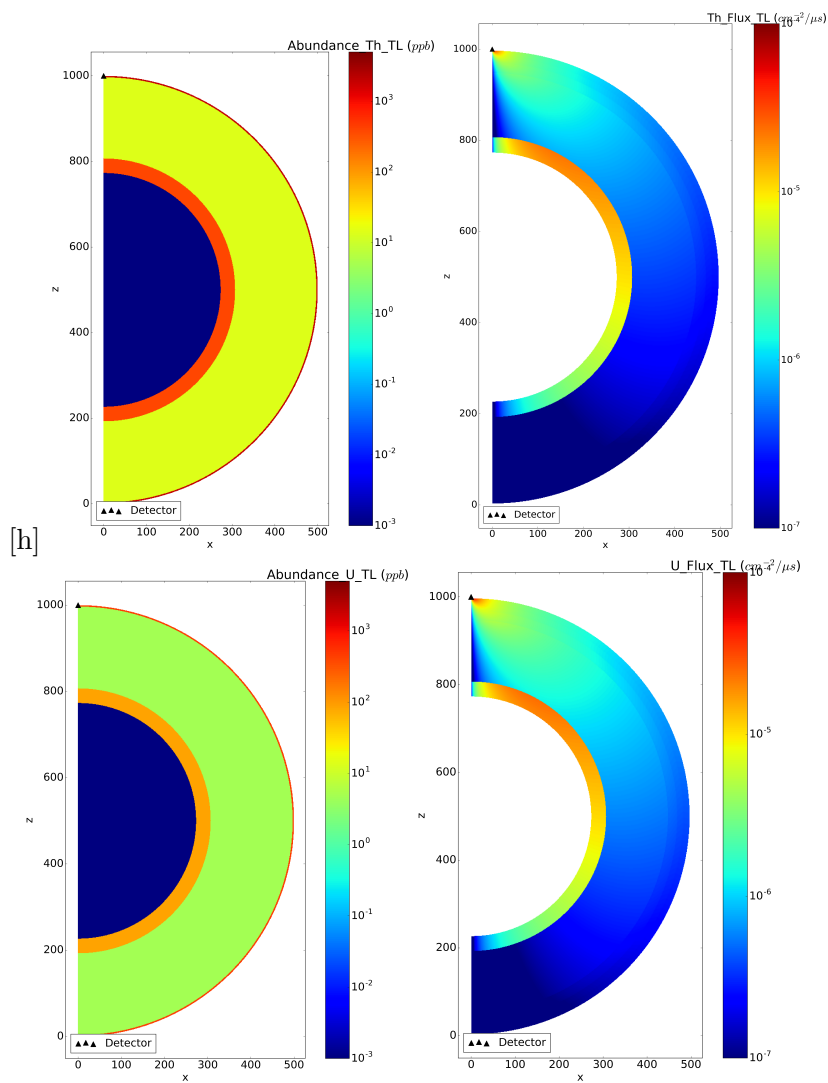


Figure 7.2: Abundance model and flux contribution for U and Th in the two-layer HPE distribution model.

# 8

## Analysis

Regarding the signal prediction, the results previously shown (specially those shown in table 7.1) are comparable to those in reference [13].

Actual measurements of geoneutrino flux have been done un KamLAND and Borexino detectors, located in Japan and Italy respectively. According to reverence [8], the measured flux values are those shown in table 8.1. For

	Borexino	KamLAND
$S_{tot}(TNU)$	$38.8 \pm 12$	$30 \pm 7$
$\Phi_{tot}(cm^{-2}/\mu s)$	$4.4 \pm 1.4$	$3.4 \pm 0.8$

Table 8.1: Experimental values for geoneutrino flux in detectors Borexino and KamLAND. Taken from reference [8].

geochemical and geodynamical BSE models, one finds a difference of about 10% between HPE distribution models, while the cosmochemical BSE leads to closer values, within 0.1% from one another; therefore, the latter might not be useful to discriminate HPE abundance models.

In figure 8.1 the mantle fluxes from  $U$  and  $Th$  are shown, in comparison to reference [13], in which the integral 6.1 is made too. In this case I used the average probability from the two.flavor approximation. In both cases, even though the simulation is close to the values given in said reference, they are not within the uncertainties there given.

On the other hand, UANdINO shows values that are, in the case of geochemical and geodynamical BSE models, way higher than expected, but the cosmochemical BSE model values are actually closer to those expected from reference [13]. The total values for the mantle expected signal in  $TNU$  are shown in figure 8.2. Reference [8] (which is easier to estimate then the mantle's) from the total. This results in a combines analysis' result for the expected mantle signal of  $7.7 \pm 6.2 TNU$ . Taking this into account, UANdINO shows results outside of the expected range in 2/3 BSE models,

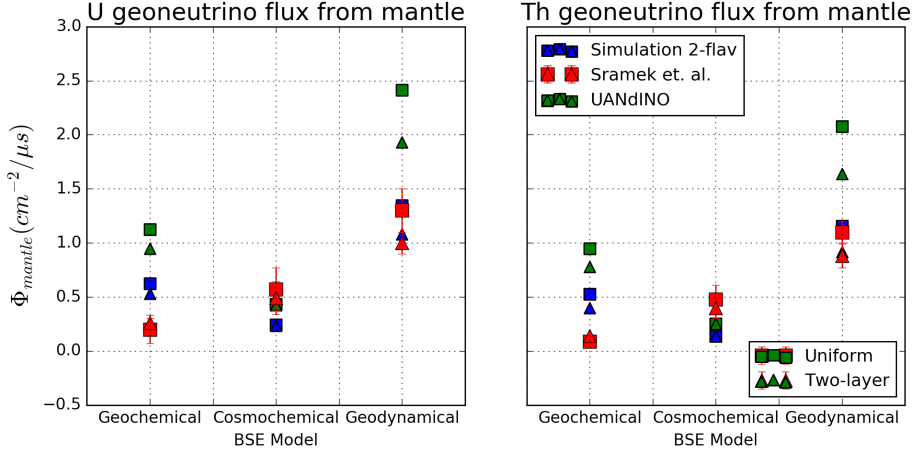


Figure 8.1: Mantle fluxes due to  $U$  (left) and  $Th$  (right), compared with those given in reference [13].

confirming what we said before.

Reference [8] also shows the results from Borexino and KamLAND detec-

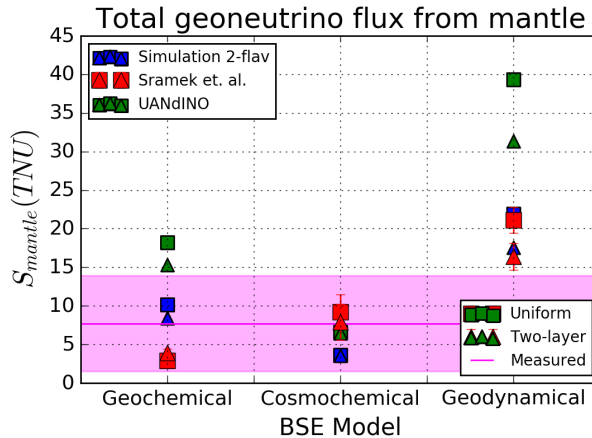


Figure 8.2: Geoneutrino signal expected from the mantle for the different models and the expected signal from detectors according to reference [8].

tors in terms of total geoneutrino flux measured. In figure 8.3 the results of both simulations (UANDINO's and two-flavor probabilities) along with the measurements of the detectors according to said reference. In this case, the UANDINO results look promising since they are within the expected in 2/3 BSE models. The results show that the geochemical BSE model fits best to the available data as seen in figure 8.3. In figure 8.2, the closest value from

UANDINO's simulation is also the geochemical BSE model. These, rather small, discrepancies can be attributed to the uncertainties in the integration of the flux, product of the discretization of the Earth. If we looked only at the two-flavor approximation, the best-fitting one is still the geochemical, since it is closer to the central value of 7.7  $TNU$ .

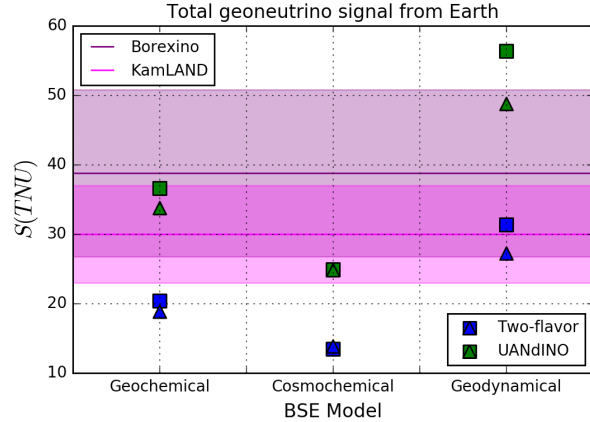


Figure 8.3: Total geoneutrino flux expected from the different models. Triangles are still two-layer and squares, uniform HPE distributions. Colored bands correspond to signals measured by the detectors according to reference [8].

# 9

## Conclusions

The main goal for this objective was to discriminate between the different HPE distribution models by using rigorous neutrino matter oscillation formalism, since this has been a debate in geoscience given the multiple models for the mantle that rely on information such as it's dynamics or heat flow product of radioactive decay. The introduction of new information coming from neutrino geoscience may be the necessary step to link the available information and draw conclusions.

First, one should look at which of the BSE models shows a better fit with the data available from the detectors. In this matter, the geochemical BSE model is the one, since in the total expected flux of figure 8.3 it seems to be an average between Borexino and KamLAND measurements. This is important since these detectors are in radically different geological settings, which is said to affect the geoneutrino flux; while the simulation is an “average” Earth. In the case of the mantle expected flux (fig. 8.2), the geochemical BSE model is also the one closer to the central value and to the “expectancy” area. The discrepancies can be attributed to uncertainties in the integration, mainly given by the discretization of the planet.

Then, regarding the HPE distributions, we can conclude that, even though the two models give rather similar results, the ones of the two-layer model can be closer to the measured values, nevertheless, the results are not entirely conclusive in this respect.

### 9.1 Further Problems

As I stated before, geoneutrinos are a rather new tool in geophysics and Neutrino Geoscience a new field in geoscience, there is a lot more work to do and problems to solve.

This project aimed to simulate the Earth in a “simple-enough” way that allowed the testing of UAndINO, the software written to exactly solve the matter-oscillation of (anti)neutrinos. Nevertheless UAndINO is not as reli-

able and fast as I would want it to be and work is to be done in this area. Another thesis project will be done for this. In particular I would have to figure out why does the probability given by the software is so different from the average one and how come it can still give “reasonable” results.

On the other hand, the Earth modelling was satisfactory, since it allowed to reproduce some of the basic properties of the planet and gave some liberties on parameters such as the HPE abundances and their distribution. Nevertheless, the mantle is known to be way more complex than the two-layer model. This model can be refined in order to include mantle heterogeneities result of convection that leads to subducting crust, thus, increasing HPE abundance in the mantle. Unfortunately, these modifications are not trivial and a big part of the software might have to be rewritten.

# References

- [1] Adam M. Dziewonski and Don L. Anderson. “Preliminary reference Earth model”. In: *Physics of the Earth and Planetary Interiors* 25.4 (1981), pp. 297–356. ISSN: 00319201. DOI: 10.1016/0031-9201(81)90046-7.
- [2] S. Enomoto. “Neutrino Geophysics and Observation of Geo-Neutrinos at KamLAND”. PhD thesis. 2005, p. 233.
- [3] Mark Galassi et al. *GNU Scientific Library Release 2.4*. 2017. URL: <https://www.gnu.org/software/gsl/doc/latex/gsl-ref.pdf>.
- [4] Carlo Giunti and Chung W. Kim. “Fundamentals of Neutrino Physics and Astrophysics”. In: *Fundamentals of Neutrino Physics and Astrophysics* (2010), pp. 1–728. ISSN: 0717-6163. DOI: 10.1093/acprof:oso/9780198508717.001.0001. arXiv: 9809069v1 [arXiv:gr-qc].
- [5] Victor Goldschmidt. *Geochemistry*. 1st ed. The Clarendon Press, 1958.
- [6] Yu Huang et al. “A reference Earth model for the heat-producing elements and associated geoneutrino flux”. In: *Geochemistry, Geophysics, Geosystems* 14.6 (2013), pp. 2003–2029. ISSN: 15252027. DOI: 10.1002/ggge.20129. arXiv: 1301.0365.
- [7] Kenneth S. Krane. *Introductory Nuclear Physics*. Wiley, 1988. ISBN: 9780471805533. DOI: 9780471805533.
- [8] L. Ludhova and S. Zavatarelli. “Studying the earth with geoneutrinos”. In: *Advances in High Energy Physics* 2013 (2013). ISSN: 16877357. DOI: 10.1155/2013/425693. arXiv: 1310.3961.
- [9] Shen-Su McDonough, William F; Sun. “The Composition of The Earth”. In: *Chemical Geology* 120 (1995), pp. 223–253. ISSN: 00092541. DOI: 10.1016/0009-2541(94)00140-4.
- [10] Scott M. McLennan. “Relationships between the trace element composition of sedimentary rocks and upper continental crust”. In: *Geochemistry, Geophysics, Geosystems* 2.4 (Apr. 2001), n/a–n/a. ISSN: 15252027. DOI: 10.1029/2000GC000109. URL: <http://doi.wiley.com/10.1029/2000GC000109>.

- [11] Tommy Ohlsson and Hakan Snellman. “Neutrino oscillations with three flavors in matter of varying density”. In: *The European Physical Journal C* 20.3 (2001), pp. 507–515. ISSN: 1434-6044. DOI: 10.1007/s100520100687. arXiv: 0103252 [hep-ph]. URL: <http://arxiv.org/abs/hep-ph/0103252%7B%5C%7D5Cnhttp://www.springerlink.com/index/10.1007/s100520100687>.
- [12] R.L. Rudnick and S. Gao. “3.01 Composition of the Continental Crust”. In: *Treatise on Geochemistry*. 2003, pp. 1–64. ISBN: 9780080437514. DOI: 10.1016/B0-08-043751-6/03016-4. URL: <http://www.sciencedirect.com/science/article/pii/B0080437516030164>.
- [13] Ondrej Sramek et al. “Geophysical and geochemical constraints on geoneutrino fluxes from Earth’s mantle”. In: *Earth and Planetary Science Letters* 361 (2013), pp. 356–366. ISSN: 0012821X. DOI: 10.1016/j.epsl.2012.11.001. arXiv: [arXiv:1207.0853v2](https://arxiv.org/abs/1207.0853v2).
- [14] Stuart Ross Taylor and Scott M. McLennan. “The geochemical evolution of the continental crust”. In: *Reviews of Geophysics* 33.2 (May 1995), p. 241. ISSN: 8755-1209. DOI: 10.1029/95RG00262. URL: <http://doi.wiley.com/10.1029/95RG00262>.
- [15] K Hans Wedepohl. “The composition of the continental crust”. In: *Geochimica et Cosmochimica Acta* 59.7 (Apr. 1995), pp. 1217–1232. ISSN: 00167037. DOI: 10.1016/0016-7037(95)00038-2. URL: <http://www.sciencedirect.com/science/article/pii/0016703795000382>.

# Index

Bulk Silicate Earth (BSE)

- cosmochemical, 8
- geochemical, 8
- geodynamical, 8

Eigenstate

- flavor, 15
- mass, 15

Goldschmidt

- classification, 7

Hamiltonian, 15

Neutrino

- definition, 15